Solar Energy Materials and Solar Cells 176 (2018) 266–272

Contents lists available at ScienceDirect

Solar Energy Materials and Solar Cells

journal homepage: www.elsevier.com/locate/solmat

Synthesis of colloidal VO_2 nanoparticles for thermochromic applications

Yongwon Choi*, Dong Min Sim, Yoon Hyung Hur, Hyeuk Jin Han, Yeon Sik Jung

Department of Materials Science and Engineering, Korea Advanced Institute of Science and Technology (KAIST), 291 Daehak-ro, Yuseong-gu, Daejeon 305-701, Republic of Korea

ARTICLE INFO

Keywords:
Thermochromic
Vanadium dioxide
Nanopatterning
Luminous transmittance

ABSTRACT

Vanadium dioxide (VO_2) thin films are key materials for thermochromic smart windows and commonly have a typical phase transition (insulator to metal phase) at a transition temperature of 68 °C. This research, however, found that highly crystallized VO_2 nanoparticles can be successfully coated on a glass substrate with added functionalities, such as higher luminous transmittance and transition efficiency. The transition temperature revealed that the VO_2 nanoparticles with post thermal treatment at 600 °C also clearly exhibited a reduced transition temperature of 69 °C in the heating curve, 59 °C in the cooling curve, and a transition width of 10 °C. By nanopatterning the thin films, we were able to prepare VO_2 thin films with higher luminous transmittance than that attained with non-patterned VO_2 thin films. The enhanced transition property was demonstrated using highly crystallized VO_2 nanoparticles induced by post thermal treatment, and the luminous transmittance was improved by the nanopatterns on the surface of the VO_2 thin films.

1. Introduction

Smart windows are currently being intensely investigated so that they can be effectively implemented in modern energy saving buildings. For smart windows, chromogenic materials have been researched for many years and a large number of practical applications have been found because of reversible changes in their optical characteristics occurred due to some external stimulus. Many chromogenic materials are reported in field of thermochromic, photochromic, and electrochromic, which are changed material properties of physical and chemical by temperature, light [1–5], and electric field [6], respectively. In particular, thermochromic windows have effectively reduced energy consumption in residential and commercial buildings because the phase transition effectively regulates the solar irradiation in a wavelength of 800–2500 nm [7–9].

Thermochromic materials are capable of a reversible change in optical transmittance and electrical resistance in response to environmental temperature. Vanadium dioxide (VO_2) is well known as one of the most promising thermochromic materials [10]. At below the transition temperature, VO_2 has a semiconductor or insulator state with a monoclinic structure. When VO_2 is heated above the transition temperature, it undergoes changes in the electrical resistance and optical transparency, particularly in the near-mid infrared wavelength regime, due to the structural change from monoclinic to tetragonal [11–13]. Because of their distinctive optical and electrical switching characteristics, VO_2 thin films hold potential to be used for a number of practical applications, including smart windows [14–16], infrared sensors or detectors [17], and Mott transistors [18].

A number of methods have been studied to fabricate VO_2 thin films with better phase transition characteristics, including physical vapour deposition (PVD) such as DC or RF reactive sputtering [19–21], ion beam assisted sputtering [22], pulsed laser deposition [23], and chemical vapour deposition (CVD) [24,25]. However, it is difficult to perform large-area deposition on the substrate and achieve low cost production due to the high process temperature. These temperatures are still too high to use soda-lime glass as a substrate for smart window applications because it is difficult to prevent ion diffusion from a soda-lime substrate. Recently, solution-based processes, such as sol-gel deposition [26], an electrochemical process [27], a hydrothermal process [28,29], and polymer-assisted deposition [30], have been used to fabricate pure VO_2 thin films to obtain high thermochromic characteristics.

Sol-gel deposition is a typical solution-based synthesis process with various chemical materials and creates a vanadium oxide network by the polymerization of chemical precursors, such as vanadyl triisopropoxide ($VO(OC_3H_7)_3$) [31], vanadium oxyacetylacetone ($VO(acac)_2$) [32], and ammonium meta-vanadate (NH_4VO_3) [33]. VO_2 nanoparticles have attracted much attention due to their size- and shape-tunable properties, which are more highly desirable for low-cost industrial production of VO_2 thin films than those produced with conventional gas phase deposition such as PVD and CVD. However, synthesized VO_2 thin films are significantly limited in their use because of a number of issues, including a relatively low luminous transmittance in

* Corresponding author.
E-mail address: choiyongwon@kaist.ac.kr (Y. Choi).

https://doi.org/10.1016/j.solmat.2017.12.008
Received 30 November 2016; Received in revised form 7 July 2017; Accepted 9 December 2017
Available online 22 December 2017

the visible regime and low transition efficiency in the solar transmittance.

In order to enhance the luminous transmittance, some researchers have introduced doping in the VO_2 thin films with fluorine (F) [34], magnesium (Mg) [35], and titanium (Ti) [36]. Another way to enhance the optical properties introduced index matching layers in the VO_2 thin films, like an anti-reflection coating with TiO_2, Al_2O_3, Nb_2O_5, or SiO_2 layers, which provide a significant enhancement in the transmittance and successfully maintain the infrared transmittance [37]. Such layering not only suppresses the reflectance in the visible wavelength regime but also shifts the peak position of the optical transmittance to the short or long wavelength region, however additional processes and materials are needed to make index matching layers.

In this paper, we describe the synthesis of colloidal VO_2 nanoparticles with a high luminous transmittance. The highly crystallized VO_2 nanoparticles exhibited a VO_2 phase through post thermal treatment. In addition, using a nanoimprinting method, we patterned the VO_2 thin films to control the aperture ratio with striped lines and spaces. We also discuss the thermochromic characteristics of the nanopatterned VO_2 thin films.

2. Experimental procedure

2.1. Synthesis of colloidal VO_2 nanoparticles

In a typical synthesis procedure, ammonium meta-vanadate (NH_4VO_3, 99%, Sigma-Aldrich) and ethylene glycol ($C_2H_6O_2$, 99.8%, Sigma-Aldrich) were used as received to prepare the vanadium precursor. To reduce or depress the aggregation of nanocrystals during synthesis, oleic acid ($C_{18}H_{34}O_2$, Sigma-Aldrich) was utilized as a structure directing agent with the VO_2 nanoparticles. As shown in Fig. 1(a), 3 g of NH_4VO_3, 3 g of oleic acid and 60 mL of $C_2H_6O_2$ were mixed in a 250 mL round-bottomed flask. The mixture was purged by N_2 gas, and then the flask was placed in a heating mantle at 160 °C under vigorous stirring. The temperature of the solution was monitored by thermocouples. The color of the reaction solution turned from yellow to blue after 60 min. The blue precipitate was washed and filtered several times with 60 mL of $C_2H_6O_2$ by a 0.1 μm pore sized PTFE membrane under reduced pressure. The filtered precipitate was placed in a convection oven at 200 °C for 30 min to remove most of the $C_2H_6O_2$ and water and to form crystalline VO_2 nanoparticles. After cooling to room temperature, the resulting particles were mixed with 10 mL of $C_2H_6O_2$ and sonicated for 10 min to form a suspension. The suspension was filtered again and the resulting precipitate was treated in a convection oven at 200 °C for 30 min [38].

2.2. Post thermal treatment

The resulting particles were further annealed in a vacuum furnace to enhance the crystallinity of the VO_2 nanoparticles. When the base pressure in the tube furnace reached 5×10^{-3} Torr, the nanoparticles were annealed at a temperature of 600 °C with different annealing times from 60 to 180 min. The annealing temperature was controlled by a temperature controller with a heating rate of about 10 °C/min. For an accurate reading of the furnace temperatures, temperature calibration was performed using K-type thermocouples directly attached to the surface of the furnace tube. The annealing atmosphere with Ar gas was kept at 50 sccm, which was precisely controlled with a mass flow controller (MFC). After thermal treatment, the VO_2 nanoparticles in ethanol were treated by ultra-sonication and syringe filtering with a 0.45 μm pore size to reduce the average size of the nanoparticles because larger particle sizes could not be used to fabricate VO_2 thin films because they could not be dispersed in the solvent.

2.3. Preparation of nanopatterned VO_2 thin film

As shown in Fig. 1(b), the nanopatterned VO_2 thin films were fabricated through a polydimethylsiloxane (PDMS) mold and spin coating. The Si trench master mold with a pattern width of 250 nm and different patterns for different pattern periods was fabricated using KrF photolithography followed by reactive ion etching (RIE). A positive photoresist with a thickness of 400 nm was spin coated on 200 mm Si wafers, which was exposed by a KrF scanner (Nikon, NSR-S203B), followed by developing using a developer solution (tetramethylammonium hydroxide, TMAH). The photoresist patterns were used as an etch mask to pattern the Si surface by reactive ion etching by CF_4 gas. After the stripping of the remaining photoresist, trench patterns with a width of 250 nm, a depth of 200 nm, and a different period were obtained and used for VO_2 nanofabrication. To fabricate the PDMS mold, pre-polymers and a curing agent (Sylgard 184, Dow Corning Co. Ltd.) were mixed with a weight ratio of 10:1, and the resulting air bubbles in the mixture were eliminated by degassing in a vacuum. The mixture was then poured on a silicon wafer and baked at 150 °C for 30 min using a convection oven. Poly-4-vinylpyridine (P4VP) film was spin coated on the elastomeric PDMS mold, which was prepared by thermal curing pre-polymers on surface-patterned silicon templates. To remove the top-

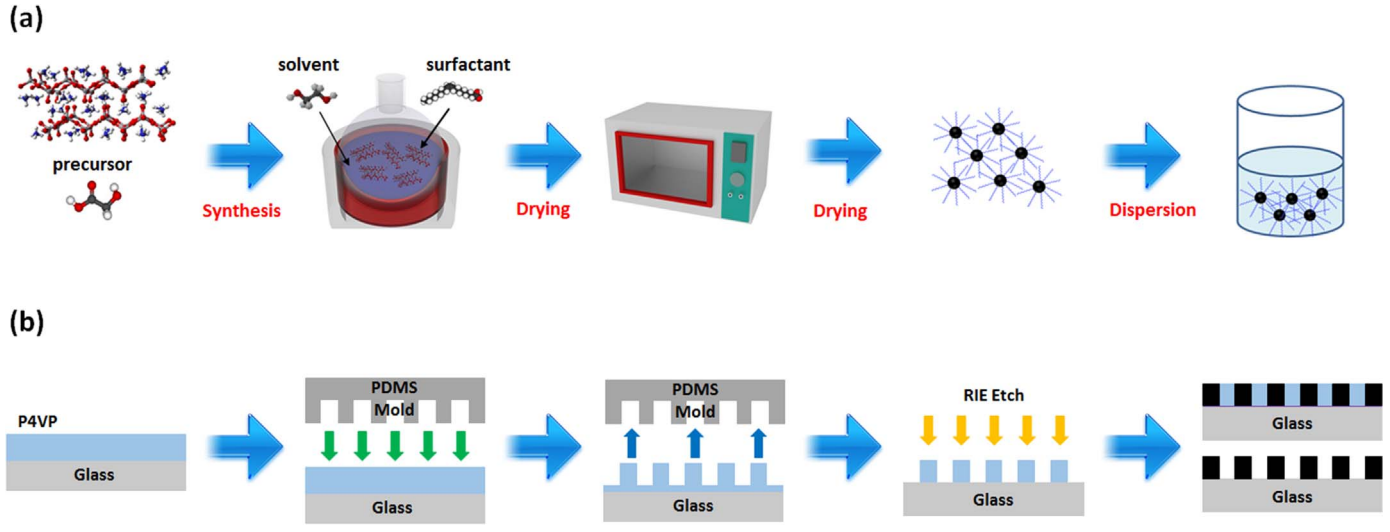

Fig. 1. A schematic of the general procedure for nanopatterned VO_2 thin films. (a) Preparation of VO_2 nanoparticles with ammonium meta-vanadate, oleic acid, and ethylene glycol. (b) Nanoimprinting method to fabricate nanopatterns by a PDMS mold.

segregated P4VP layer and organic blocks, the samples were etched by oxygen plasma (etching time = 20 s, O_2 gas flow rate = 30 sccm, working pressure = 15 mTorr, plasma source power = 100 W, and substrate bias power = 50 W). After a short treatment of oxygen plasma that removed the residual bottom polymer layers, 200 nm of nanopatterns with different pattern periods were formed on a glass substrate. The glass substrate (Corning® EAGLE XG®) with a thickness of 0.7 mm was cleaned by isopropyl alcohol and dried with N_2 gas and then exposed to an ozone cleaner for 10 min. Aperture ratios with striped lines and spaces were kept at 17%, 34%, and 50%. To fabricate VO_2 thin films, the VO_2 nanoparticles were dispersed in ethanol to form a homogeneous solution with ethanol (10 mL) and VO_2 nanoparticles (1 mg). The VO_2 nanoparticles were treated by syringe filtering with a 0.45 μm pore size and ultra-sonication to reduce the average particle sizes. The thin films were coated on nanopatterned glass by spin coating with 0.4 mg of solution at a high speed of 1500 rpm for 15 s.

2.4. Characterization

Structural analysis of the VO_2 particles was performed using high resolution powder X-ray diffraction (XRD, smartLab, Rigaku) with Cu-K_α radiation (λ = 1.5405 Å) generated at 40 kV and 30 mA. To verify the thermochromic behavior of the VO_2 thin films, the transmittance spectra with a 0° incident angle were measured using a UV–vis spectrophotometer (V-670, JASCO) in a wavelength region of 300–2500 nm at two different temperatures, 20 °C and 90 °C. The sample stage could be used to vary the temperature in a range of 20–100 °C with a heating and cooling rate of about 1 °C/min, based on the Peltier effect. The integral luminous transmittance (T_{lum}) in a wavelength of 380–780 nm and the solar transmittance (T_{sol}) in a wavelength of 300–2500 nm were calculated from $T_{lum,sol} = \int \varphi_{lum,sol}(\lambda)T(\lambda)d\lambda \,/\, \int \varphi_{lum,sol}(\lambda)d\lambda$, where φ_{lum} is the spectral sensitivity of the light-adapted eyes and φ_{sol} is the solar irradiation spectrum for an air mass of 1.5 (corresponding to the sun standing 37° above the horizontal). ΔT_{sol} refers to the difference in the average optical transmittance levels in a wavelength range of 300–2500 nm between 20 °C and 90 °C, which was obtained from ΔT_{sol} = (T_{sol} at the 20 °C) − (T_{sol} at the 90 °C) [39]. The microstructures of VO_2 nanoparticles were investigated by field emission scanning electron microscopy (FE-SEM, S-4800, Hitachi) with an acceleration voltage of 10 kV and high resolution transmission electron microscopy (HRTEM, JEM-2100F, JEOL) with an acceleration voltage of 200 kV, respectively. The transition temperature in the VO_2 nanoparticles was investigated by low temperature differential scanning calorimetry (DSC, DSC204F1, NETZSC). The sample was placed in a N_2 gas flow in a temperature range of 20–100 °C with a heating and cooling rate of about 5 °C/min. Resistance measurements were performed on 1 cm × 1 cm sized VO_2 thin films on a glass substrate. The two contact pad was fabricated by an e-beam evaporator with Ag-plated electrodes. The resistance was measured by a probe station (Keithley 4200-SCS, MST-1000H, MSTECH). The chemical composition between oleic acid and VO_2 nanoparticles was measured by Fourier transform infrared spectroscopy (FT-IR, IFS66V/S, Bruker). The KBr pellets were prepared by pressing 500 mg of VO_2 nanoparticles under a pressure of 15 MPa, which was measured in a spectra range from 4000 to 400 cm^{-1}.

3. Results and discussions

The structural change in the VO_2 nanoparticles with different synthesis conditions and their crystal and surface morphologies were examined by the XRD, SEM, and TEM, respectively. Fig. 2(a) shows that the XRD patterns for the as-synthesized vanadyl ethylene glycolate (VEG), and VO_2 nanoparticles in a convection oven at 160 °C for 60 min and 120 min were well indexed in terms of the VEG (*C*2/c, JCPDS card number: #49-2497) and VO_2 monoclinic lattice ($P2_1/c$, JCPDS card number: #43-1051). Thermolysis indicated that the VO_2 nanoparticles were mostly composed of a crystalline VO_2 phase with a preferred (011) orientation at 2θ = 27.90° and the other peaks of the spectrum at 2θ = 37.07°, 42.21°, 55.53°, and 57.54° corresponded to the (200), (−212), (211), and (022) plane of the VO_2, respectively [40]. As the time of thermolysis increased, the peak intensity of the (011) orientation and other orientations, (200), (−212), (211), and (022), in the VO_2 nanoparticles slightly increased and the peak width of the full width half maximum (FWHM) also decreased. However, we ascribed a low intensity peak at around 25–27° for the VO_2 nanoparticles to the presence of a V_6O_{13} phase. The formation of these unwanted crystal phases might have been caused by excessive oxidation during the drying with as-synthesized VEG in the oven. The average crystal sizes were calculated from the (011) peaks of the VO_2 nanoparticles by applying Scherrer's formula on the XRD patterns, $D = K\lambda / (\beta \cos\theta)$, where D is the mean size of crystallites (nm), K is a dimensionless shape factor that has a typical value of about 0.94, λ is the X-ray wavelength (1.5405 Å), β is the full width at half the maximum (FWHM) in radians of the X-ray diffraction peak and θ is Braggs' angle. The crystal sizes were 29.5 nm at 160 °C for 60 min and 34.2 nm at 160 °C for 120 nm.

The SEM images for the pure VO_2 nanoparticles without a surfactant are shown in Fig. 2(b). The VO_2 nanoparticles consisted of an amount of long ranged nanorods and an aggregated structure below 500 nm. According to the TEM images (see in Fig. 2(c)), the crystallite structures were spherical with 20–30 nm diameters. The crystal sizes were in good agreement with the results of the XRD patterns.

Fig. 3(a) and (b) show the structure of the VO_2 nanoparticles with/without oleic acid as a surfactant. The surface treated VO_2 nanoparticles were better dispersed in ethanol compared with oleic acid-free VO_2 nanoparticles. To apply VO_2 nanoparticles in various potential applications, it is very important to control their size and shape as well as dispersion properties by surface modification. Oleic acid is a commonly used surfactant for stabilizing the synthesized nanoparticles. As-synthesized VO_2 nanoparticles have many defects on the surface that hinder electron transport during the phase transition. The ligand structure of the surfactant on the surface of the VO_2 nanoparticles can be arranged by their orientation and surface energy due to the hydrophilic surface combined with the surfactant [41]. In addition, the ligand reaction with VO_2 nanoparticles prevents aggregation among particles caused by surface properties of the hydrophilic surface, which sustains smaller particle sizes. As a result, the surfactant treated VO_2 nanoparticles are much smaller than surfactant-free VO_2 nanoparticles. It has also been found that the precursor solution with oleic acid treated VO_2 nanoparticles and solvent, such as ethanol or methanol, remained stable without any agglomeration for 5 days. As shown in Fig. 3(c), the FT-IR spectra of the with/without oleic acid as a surfactant and VO_2 nanoparticles on the KBr pellets in the spectra ranged from 4000 to 400 cm^{-1}. When oleic acid was injected into the synthesis with ammonium meta-vanadate and ethylene glycol, a C–H vibration was strongly detected in the VO_2 nanoparticles. Oleic acid is a commonly used surfactant in the various synthesis process because of relatively high boiling temperature of 268 °C. The absorption peak near a wavenumber of 2919 and 2838 cm^{-1} corresponded to the C–H vibration of oleic acid and the strong C=O= stretch of the oleic acid was also observed near a wavenumber of 1731, 1704, and 1554 cm^{-1}, respectively. Many researchers have already reported that they used oleic acid to make various nanoparticles [42–44]. They also investigated the chemical reaction between the surfactant and the nanoparticles at the interface by FT-IR spectra, which showed some sharp bands at 2922 and 2853 cm^{-1} in the C–H stretch spectral region and the peaks at 1743 and 1707 cm^{-1} in the C=O= stretch, respectively.

To distinguish the effect of the post thermal treatment of VO_2 nanoparticles with oleic acid as a surfactant, the VO_2 nanoparticles were annealed in a vacuum furnace by varying the annealing times from 60 min to 180 min while the temperature was kept at 600 °C. It could be seen that all the annealed VO_2 nanoparticles exhibited strong diffraction peaks at 2θ = 27.90°, 37.07°, 42.21°, 55.53°, and 57.54° corresponding to a preferred (011) orientation, (200), (−212), (211), and

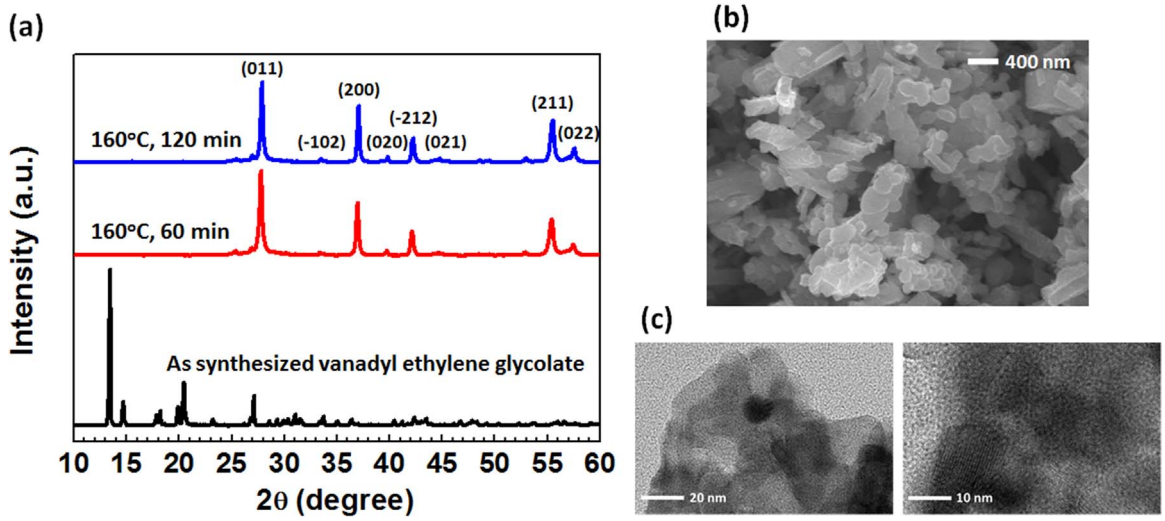

Fig. 2. The microstructure of VO_2 nanoparticles with different synthesis temperatures from 60 min to 120 min at 160 °C. (a) XRD patterns of VO_2 nanoparticles and vanadyl ethylene glycolate synthesized at 160 °C for 60 min and 120 min (b), (c) SEM and TEM images of VO_2 nanoparticles synthesized at 160 °C for 120 min.

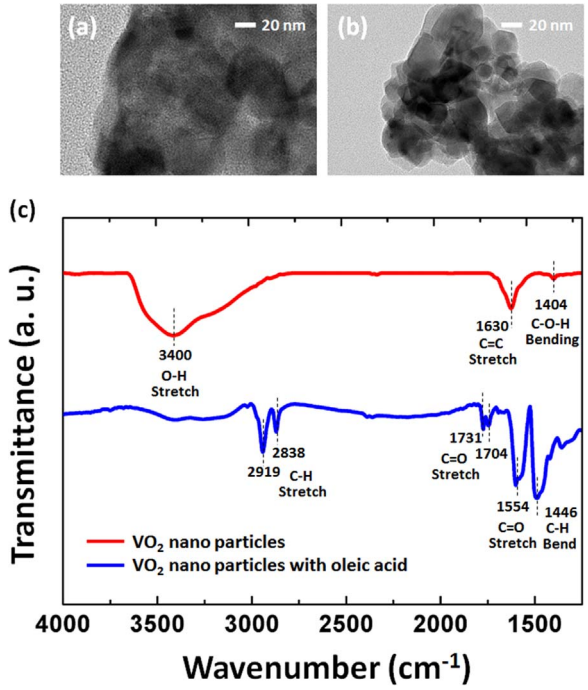

Fig. 3. TEM images of VO_2 nanoparticles with a surfactant. (a) The plane views of the VO_2 nanoparticles without a surfactant, (b) oleic acid added VO_2 nanoparticles, (c) FT-IR spectra of VO_2 nanoparticles dispersed in a KBr pellet.

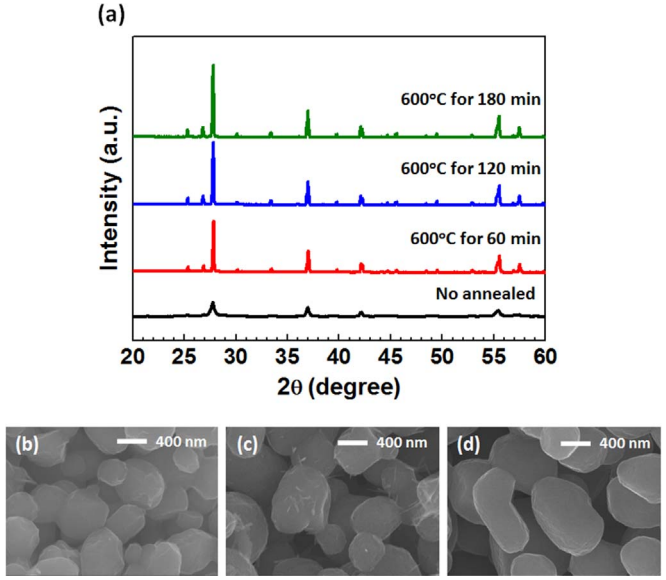

Fig. 4. (a) XRD patterns of VO_2 nanoparticles with different post thermal treatment times from 60 to 180 min while the atmosphere and temperature were kept at an Ar gas flow rate of 50 sccm and a temperature of 600 °C. SEM images of VO_2 nanoparticles with various post treatment times (b) 60 min; (c) 120 min; (d) 180 min.

(022) plane of the VO_2, respectively, which confirmed that crystalline VO_2 was successfully fabricated after post thermal annealing. The crystallinity of the VO_2 nanoparticles were affected not only by the different crystal orientation of the VO_2 nanoparticles but also by the different peak intensity. However, other kinds of diffraction peaks were also exhibited at around $2\theta = 25.36^\circ$ and 26.86°, corresponding to V_6O_{13}, probably because of excessive oxidation of V_4^+ during the post thermal treatment. Even though the unwanted crystal peaks existed at around $2\theta = 25–26^\circ$, the peak widths (FWHM) of the (011) plane gradually decreased from 0.12 to 0.11°, and the average crystallite sizes calculated from the (011) planes of the VO_2 nanoparticles increased from 74 to 78 nm as the annealing time increased from 60 to 180 nm. The trend of the average crystallite size expected from the XRD peak widths for the VO_2 nanoparticles with the different post treatment times was in agreement with the SEM results in Fig. 4(b)–(d). The VO_2 nanoparticles were composed of smaller crystallite sizes (a few tens of nanometers in size) and exhibited larger FWHMs prior to post thermal treatment (see in Fig. 2) [45–47]. After the thermal treatment with different times, the VO_2 nanoparticles had larger crystallite sizes and higher crystallinity. The average particle sizes shown in the SEM images were larger than the average crystallite sizes calculated from the XRD results. The particle size did not seem to represent the single crystallites and were likely formed by agglomeration of crystallites, but the tendency of particle sizes was similar to that of the crystal sizes. The larger particle sizes in the VO_2 nanoparticles with longer post thermal treatment can promote particle growth and enhance the crystallization of VO_2 nanoparticles [48].

The reversible phase transition of the VO_2 nanoparticles with oleic acid as a surfactant were clearly revealed by differential scanning calorimetry (DSC). As shown in Fig. 5(a), the endothermal and exothermal peaks during the heating and cooling process confirms the first-order phase transition from monoclinic to tetragonal in response to temperature. An endothermal peak was observed at 69 °C in the heating

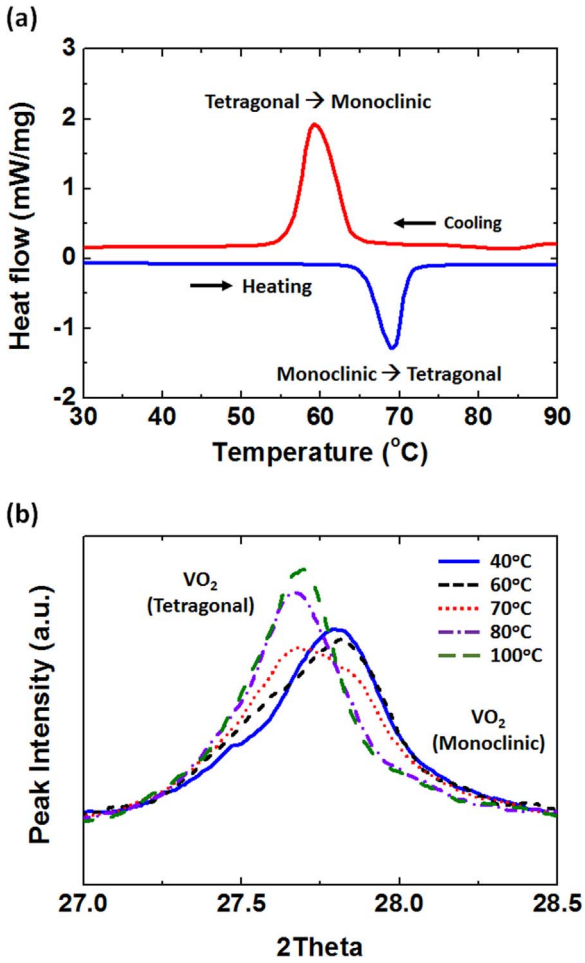

Fig. 5. Phase transition behavior of thermal annealed VO_2 nanoparticles (a) DSC curves of the post thermally treated VO_2 nanoparticles with heating/cooling rates of 5 °C/min from 30 °C to 90 °C, (b) in-situ XRD patterns according to the ambient temperature from 40 °C to 100 °C. The crystal phase of the VO_2 nanoparticles gradually changed from a monoclinic structure to a tetragonal structure.

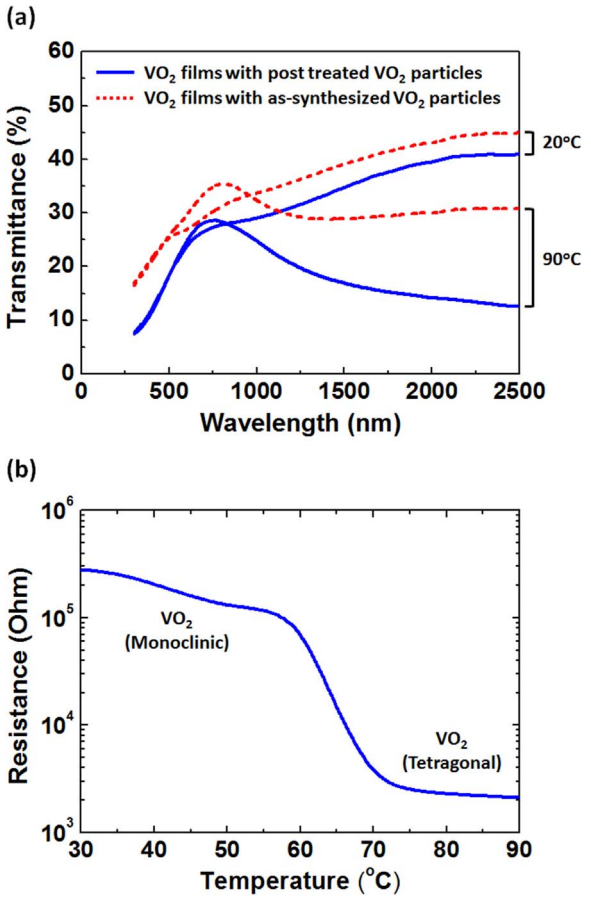

Fig. 6. Thermochromic performance of VO_2 thin films prepared by (a) as-synthesized VO_2 nanoparticles and post thermally treated VO_2 nanoparticles at 600 °C for 120 min. (b) Electrical resistance of the VO_2 thin films prepared by the post thermally treated VO_2 nanoparticles at 600 °C for 120 min.

curve of the DSC, which indicated the phase transition from a monoclinic structure to a tetragonal structure. On the other hand, the reverse phase transition from the tetragonal structure to the monoclinic structure occurred with an exothermal peak at 59 °C in the cooling curve [49]. The transition width was calculated by the difference between the heating and cooling curves in the DSC result, where the transition width was 10 °C. In addition, the phase transition behaviors were investigated by in-situ XRD for the VO_2 nanoparticles. Furthermore, the distinctive phase transition from monoclinic to tetragonal structure was verified from the in-situ XRD shown in Fig. 5(b). The crystal phase of the VO_2 nanoparticles was at a preferred (011) orientation at $2\theta = 27.90^{\circ}$, and the peaks gradually shifted to a lower angle as the ambient temperature increased from 40 °C to 100 °C, which revealed that the transition temperature by in-situ XRD was in good agreement with the result of the DSC. The phase transition from monoclinic to tetragonal structure happened in a temperature range from 60 to 70 °C in the in-situ XRD.

As shown in Fig. 6(a), both VO_2 thin films exhibited thermochromic characteristics at low (20 °C) and high (90 °C) temperature transmittance spectra. The VO_2 thin films were composed of post thermally treated VO_2 nanoparticles with a temperature of 600 °C for 120 min and as-synthesized nanoparticles. The luminous transmittance of the VO_2 thin films with post thermally treated VO_2 nanoparticles drastically increased from 21.1% to 33.6%. In addition, the transition efficiency also improved from 1.5% to 3.8%. Thus, the results confirmed that the post thermal treatment of VO_2 nanoparticles effectively improved the transition efficiency due to a higher crystallinity in the VO_2 nanoparticles. Fig. 6(b) shows the variation in the electrical resistance of the VO_2 thin films by thermally treated VO_2 nanoparticles. The value of the electrical resistance of the VO_2 thin film at 20 °C was about 10^5–10^6 Ω. On the other hand, the electrical resistance of VO_2 thin films above the transition temperature decreased to several 10^3 Ω, which demonstrated a variation of electrical resistance on the order of 10^3 Ω, as measured between 20 °C and 90 °C. That means that the phase structure of the VO_2 thin films effectively changed from monoclinic to tetragonal above the transition temperature.

The luminous transmittance of the non-patterned VO_2 thin films was limited by the reflection and absorption of light at the surface of the VO_2 thin films. To fabricate the nanopatterns of VO_2 thin films, we used in nanoimprinting method to form fine patterns on the glass substrate (see in Fig. 1(b)). The nanopatterned VO_2 thin films were fabricated by the PDMS mold of a pattern width of 250 nm with different pattern periods, for which the aperture ratio was varied from 0% to 50% according to the pattern to pattern period. The thermochromic properties as a function of aperture ratios are shown in Fig. 7. As the aperture ratio of the VO_2 thin films increased from 0% to 50%, the luminous transmittance gradually increased from 21.5% to 31.8% because the vertically aligned incident light against the glass substrate was transmitted through the non-patterned area of the VO_2 thin films [50,51]. We attributed to improvement in luminous transmittance to a decrease in the reflection and absorption on the surface of the non-patterned area like the surface of glass. Even though the luminous transmittance increased approximately 47% in the nanopatterned VO_2 thin films, the transition efficiency in the solar transmittance decreased from 4.2% to 0.1% as

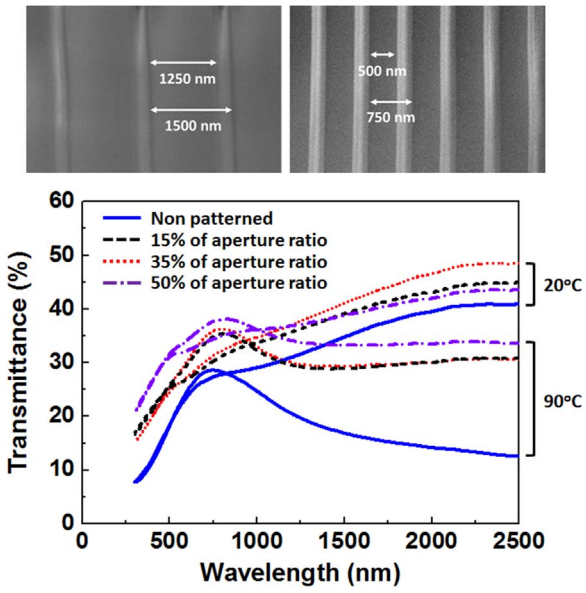

Fig. 7. Thermochromic performance of VO_2 thin films of the patterned and non-patterned thin films. The aperture ratio was controlled by the pattern to pattern periods, which was maintained 0%, 17%, 34%, and 50%.

the aperture ratio increased from 0% to 50%. The relationship between the aperture ratio of the VO_2 thin films and the transition efficiency or the luminous transmittance expressed a clearly linear relationship.

4. Conclusion

In this research, we investigated the thermochromic properties, the crystallinity, and the microstructure of vanadium dioxide (VO_2) nanoparticles synthesized with ammonium meta-vanadate and ethylene glycol by thermolysis. The solution-based synthesized VO_2 nanoparticles were well indexed in terms of the VO_2 crystal phase, which was mostly composed of a crystalline VO_2 phase with a preferred (011) orientation. The crystal sizes were estimated as 20–30 nm from the XRD and TEM images. The VO_2 nanoparticles were treated with a surfactant of oleic acid to enhance the dispersity in the solvent, which controlled the particle sizes due to the surface energy of the VO_2 nanoparticles. The post thermally treated VO_2 nanoparticles demonstrated a larger crystallite size and higher crystallinity. The highly packed, larger particles observed in the post thermally treated VO_2 nanoparticles contributed to the enhanced electron transport in the nanoparticles and led to enhanced transition characteristics. The XRD and DSC results revealed a reversible phase transition in the VO_2 nanoparticles. The phase transition from monoclinic to tetragonal was observed at 69 °C in the heating curve and the reversible phase transition occurred at 59 °C in the cooling curve. In addition, structural changes from monoclinic to tetragonal were observed in the XRD result with a temperature range from 60 to 70 °C.

The nanopatterned VO_2 thin films were fabricated by a PDMS mold with VO_2 nanoparticles were dispersed in ethanol. The VO_2 thin films were spin coated and mostly showed the crystalline diffraction peaks of the VO_2 phase. As the aperture ratio of the VO_2 thin films increased from 0% to 50%, the luminous transmittance gradually increased from 21.5% to 31.8% because most of the vertically aligned incident light was transmitted on the non-patterned area. Hence, these findings demonstrate that nanopatterned VO_2 thin films can be employed to fabricate highly luminous transmittance on glass substrates at a relatively low temperature, which is desirable for low-cost industry manufacturing.

References

[1] M.-C. Yang, H.-W. Cho, J.-J. Wu, Fabrication of stable photovoltachromic cells using a solvent-free hybrid polymer electrolyte, Nanoscale 6 (2014) 9541–9544.
[2] F. Bella, S. Galliano, C. Gerbaldi, G. Viscardi, Cobalt-based electrolytes for dye-sensitized solar cells: recent advances towards stable devices, Energies 9 (2016) 1–22.
[3] F. Bella, G. Griffini, J.-P. Correa-Baena, G. Saracco, M. Grätzel, A. Hagfeldt, T. Stefano, G. Claudio, Improving efficiency and stability of perovskite solar cells with photocurable fluoropolymers, Science 354 (2016) 203–206.
[4] F. Bella, G. Leftheriotis, G. Griffini, G. Syrrokostas, S. Turri, M. Grätzel, G. Claudio, A new design paradigm for smart windows: photocurable polymers for quasi-solid photoelectrochromic devices with excellent long-term stability under real outdoor operating conditions, Adv. Funct. Mater. 26 (2016) 1127–1137.
[5] J.-J. Wu, M.-D. Hsieh, W.-P. Liao, W.-T. Wu, J.-S. Chen, Fast-switching photovoltachromic cells with tunable transmittance, ACS Nano 3 (2009) 2297–2303.
[6] E. Syrrakou, S. Papaefthimiou, P. Yianoulis, Eco-efficiency evaluation of a smart window prototype, Sci. Total Environ. 359 (2006) 267–282.
[7] P. Jin, S. Tanemura, Formation and thermochromism of VO_2 films deposited by RF magnetron sputtering at low substrate temperature, Jpn. J. Appl. Phys. 33 (1994) 1478–1483.
[8] M. Saeli, C. Piccirillo, I.P. Parkin, R. Binions, I. Ridley, Energy modelling studies of thermochromic glazing, Energy Buildings 42 (2010) 1666–1673.
[9] M.E. Warwick, R. Binions, Chemical vapour deposition of thermochromic vanadium dioxide thin films for energy efficient glazing, J. Solid State Chem. 214 (2014) 53–66.
[10] P. Kiria, G. Hyettb, R. Binionsa, Solid state thermochromic materials, Adv. Mater. Lett. 1 (2010) 86–105.
[11] V. Eyert, The metal-insulator transitions of VO_2: a band theoretical approach, Ann. Phys. 11 (2002) 650–702.
[12] J.B. Goodenough, The two components of the crystallographic transition in VO_2, J. Solid State Chem. 3 (1971) 490–500.
[13] K. Okimura, J. Sakai, Changes in lattice parameters of VO_2 films grown on c-plane Al_2O_3 substrates across metal–insulator transition, Jpn. J. Appl. Phys. 48 (2009) 045504.
[14] Y. Gao, H. Luo, Z. Zhang, L. Kang, Z. Chen, J. Du, M. Kanehira, C. Cao, Nanoceramic VO_2 thermochromic smart glass: a review on progress in solution processing, Nano Energy 1 (2012) 221–246.
[15] C.-G. Granqvist, P. Lansåker, N. Mlyuka, G. Niklasson, E. Avendano, Progress in chromogenics: new results for electrochromic and thermochromic materials and devices, Sol. Energy Mater. Sol. Cells 93 (2009) 2032–2039.
[16] M. Kamalisarvestani, R. Saidur, S. Mekhilef, F. Javadi, Performance, materials and coating technologies of thermochromic thin films on smart windows, Renew. Sustain. Energy Rev. 26 (2013) 353–364.
[17] E. Strelcov, Y. Lilach, A. Kolmakov, Gas sensor based on metal – insulator transition in VO_2 nanowire thermistor, Nano lett. 9 (2009) 2322–2326.
[18] M. Nakano, K. Shibuya, D. Okuyama, T. Hatano, S. Ono, M. Kawasaki, Y. Iwasa, Y. Tokura, Collective bulk carrier delocalization driven by electrostatic surface charge accumulation, Nature 487 (2012) 459–462.
[19] C. Batista, R. Ribeiro, J. Carneiro, V. Teixeira, DC sputtered W-doped VO_2 thermochromic thin films for smart windows with active solar control, J. Nanosci. Nanotechnol. 9 (2009) 4220–4226.
[20] M.S. de Castro, C.L. Ferreira, R.R. de Avillez, Vanadium oxide thin films produced by magnetron sputtering from a V_2O_5 target at room temperature, Infrared Phys. Technol. 60 (2013) 103–107.
[21] Y. Shigesato, M. Enomoto, H. Odaka, Thermochromic VO_2 films deposited by RF magnetron sputtering using V_2O_3 or V_2O_5 targets, Jpn. J. Appl. Phys. 39 (2000) 6016–6024.
[22] J. Li, N. Yuan, Temperature sensitivity of resistance of VO_2 polycrystalline films formed by modified ion beam enhanced deposition, Appl. Surf. Sci. 233 (2004) 252–257.
[23] D. Fu, K. Liu, T. Tao, K. Lo, C. Cheng, B. Liu, R. Zhang, H.A. Bechtel, J. Wu, Comprehensive study of the metal-insulator transition in pulsed laser deposited epitaxial VO_2 thin films, J. Appl. Phys. 113 (2013) 043707.
[24] C. Piccirillo, R. Binions, I.P. Parkin, Synthesis and functional properties of vanadium oxides: V_2O_3, VO_2, and V_2O_5 deposited on glass by aerosol-assisted CVD, Chem. Vap. Depos. 13 (2007) 145–151.
[25] D. Vernardou, D. Louloudakis, E. Spanakis, N. Katsarakis, E. Koudoumas, Thermochromic amorphous VO_2 coatings grown by APCVD using a single-precursor, Sol. Energy Mater. Sol. Cells 128 (2014) 36–40.
[26] D. Li, W. Huang, L. Song, Q. Shi, Thermal stability of VO_2 thin films deposited by sol–gel method, J. Sol–Gel Sci. Technol. 75 (2015) 189–197.
[27] A. Cezar, I. Graff, Y. Rikers, W. Schreiner, N. Mattoso, Highly oriented VO_2 thin films prepared by electrodeposition, Electrochem. Solid State Lett. 14 (2011) 23–25.
[28] D. Alie, L. Gedvilas, Z. Wang, R. Tenent, C. Engtrakul, Y. Yan, S.E. Shaheen, A.C. Dillon, C. Ban, Direct synthesis of thermochromic VO_2 through hydrothermal reaction, J. Solid. State. Chem. 212 (2014) 237–241.
[29] S.R. Popuri, M. Miclau, A. Artemenko, C. Labrugere, A. Villesuzanne, M.l. Pollet, Rapid hydrothermal synthesis of VO_2 (B) and its conversion to thermochromic VO_2 (M1), Inorg. Chem. 52 (2013) 4780–4785.
[30] L.T. Kang, Y.F. Gao, H.J. Luo, VO_2 films by polymer-assisted deposition: investigation of thermal decomposition of precursor gel and control of phase transition temperatures, Mater. Sci. Forum Trans Tech Publ. (2011) 791–797.
[31] C.B. Greenberg, Undoped and doped VO_2 films grown from $VO(OC_3H_7)_3$, Thin Solid

Films 110 (1983) 73–82.
[32] Z. Zhang, Y. Gao, Z. Chen, J. Du, C. Cao, L. Kang, H. Luo, Thermochromic VO_2 thin films: solution-based processing, improved optical properties, and lowered phase transformation temperature, Langmuir 26 (2010) 10738–10744.
[33] G. Nagabhushana, G. Chandrappa, Facile solution combustion synthesis of monoclinic VO_2: a unique and versatile approach, J. Mater. Chem. A 1 (2013) 11539–11542.
[34] W. Burkhardt, T. Christmann, S. Franke, W. Kriegseis, D. Meister, B. Meyer, W. Niessner, D. Schalch, A. Scharmann, Tungsten and fluorine co-doping of VO_2 films, Thin Solid Films 402 (2002) 226–231.
[35] J. Zhou, Y. Gao, X. Liu, Z. Chen, L. Dai, C. Cao, H. Luo, M. Kanahira, C. Sun, L. Yan, Mg-doped VO_2 nanoparticles: hydrothermal synthesis, enhanced visible transmittance and decreased metal–insulator transition temperature, Phys. Chem. Chem. Phys. 15 (2013) 7505–7511.
[36] M. Nishikawa, T. Nakajima, T. Kumagai, T. Okutani, T. Tsuchiya, Ti-doped VO_2 films grown on glass substrates by excimer-laser-assisted metal organic deposition process, Jpn. J. Appl. Phys. 50 (2011) 01BE04.
[37] N. Mlyuka, G. Niklasson, C.-G. Granqvist, Thermochromic multilayer films of VO_2 and TiO_2 with enhanced transmittance, Sol. Energy Mater. Sol. Cells 93 (2009) 1685–1687.
[38] N. Wang, S. Magdassi, D. Mandler, Y. Long, Simple sol–gel process and one-step annealing of vanadium dioxide thin films: synthesis and thermochromic properties, Thin Solid Films 534 (2013) 594–598.
[39] Z. Chen, Y. Gao, L. Kang, J. Du, Z. Zhang, H. Luo, H. Miao, G. Tan, VO_2-based double-layered films for smart windows: optical design, all-solution preparation and improved properties, Sol. Energy Mater. Sol. Cells 95 (2011) 2677–2684.
[40] J. Zou, Y. Peng, H. Lin, A low-temperature synthesis of monoclinic VO_2 in an atmosphere of air, J. Mater. Chem. A 1 (2013) 4250–4254.
[41] Y. Xu, W. Huang, Q. Shi, Y. Zhang, J. Wu, L. Song, Porous nano-structured VO_2 films with different surfactants: synthesis mechanisms, characterization, and applications, J. Mater. Sci.-Mater. Electron. 24 (2013) 3823–3829.
[42] L. Zhang, R. He, H.-C. Gu, Oleic acid coating on the monodisperse magnetite nanoparticle, Appl. Surf. Sci. 253 (2006) 2611–2617.
[43] X. Teng, H. Yang, Effects of surfactants and synthetic conditions on the sizes and self-assembly of monodisperse iron oxide nanoparticles, J. Mater. Chem. 14 (2004) 774–779.
[44] A.G. Young, N. Al-Salim, D.P. Green, A.J. McQuillan, Attenuated total reflection infrared studies of oleate and trioctylphosphine oxide ligand adsorption and exchange reactions on CdS quantum dot films, Langmuir 24 (2008) 3841–3849.
[45] J. Wu, W. Huang, Q. Shi, J. Cai, D. Zhao, Y. Zhang, J. Yan, Effect of annealing temperature on thermochromic properties of vanadium dioxide thin films deposited by organic sol–gel method, Appl. Surf. Sci. 268 (2013) 556–560.
[46] L. Kang, Y. Gao, Z. Zhang, J. Du, C. Cao, Z. Chen, H. Luo, Effects of annealing parameters on optical properties of thermochromic VO_2 films prepared in aqueous solution, J. Phys. Chem. C 114 (2010) 1901–1911.
[47] H. Zhang, Z. Wu, X. Wu, W. Yang, Y. Jiang, Transversal grain size effect on the phase-transition hysteresis width of vanadium dioxide films comprising spheroidal nanoparticles, Vacuum 104 (2014) 47–50.
[48] Z. Lu, C. Li, Y. Yin, Synthesis and thermochromic properties of vanadium dioxide colloidal particles, J. Mater. Chem. 21 (2011) 14776–14782.
[49] Y. Sun, S. Jiang, W. Bi, R. Long, X. Tan, C. Wu, S. Wei, Y. Xie, New aspects of size-dependent metal-insulator transition in synthetic single-domain monoclinic vanadium dioxide nanocrystals, Nanoscale 3 (2011) 4394–4401.
[50] S.-H. Hong, J. Hwang, H. Lee, Replication of cicada wing's nano-patterns by hot embossing and UV nanoimprinting, Nanotechnology 20 (2009) 385303.
[51] S.H. Lee, J.W. Leem, J.S. Yu, Transmittance enhancement of sapphires with anti-reflective subwavelength grating patterned UV polymer surface structures by soft lithography, Opt. Express 21 (2013) 29298–29303.